

Through-thickness permeability modelling of woven fabric under out-of-plane deformation

Xueliang Xiao · Andrew Long · Xuesen Zeng

Received: 28 March 2014 / Accepted: 10 July 2014 / Published online: 30 July 2014
© Springer Science+Business Media New York 2014

Abstract When a woven fabric is subject to a normal uniform loading, its properties such as tightness and through-thickness permeability are both altered, which relates to the fabric out-of-plane deformation (OPD) and dynamic permeability (DP). In this article, fabric OPD is analytically modelled through an energy minimisation method, and corresponding fabric DP is established as the function of loading and fabric-deformed structure. The total model shows the permeability a decrease for tight fabric and an increase for loose fabric when the uniform loading increases. This is verified experimentally by fabric OPD, static and dynamic permeabilities. Experimental tests for both permeabilities showed good agreement with the corresponding predictions, indicating the fact that tight fabric becomes denser and loose fabric gets more porous during OPD. A sensitivity study showed that an increase of fabric Young's modulus or a decrease of fabric test radius both lead to an increase of DP for tight fabric and opposite for loose fabric. The critical fabric porosity and thickness were found for inflexion of fabric DP trend during the OPD, which contributes to the optimum design of interlacing structure applied to protective textiles and composites.

Introduction

Many technical textiles during bulking, such as inflation of airbag and artificial blood vessel, are subject to pressure loading perpendicular to the fabric in-planar. The perpendicular loading easily causes the interlacing structural fabric a deformed out-of-plane curved profile. The transient permeability and the subsequent protective effect and transport efficiency are thereafter varied dynamically during the deformation. Therefore, it is important to model this fabric out-of-plane deformation (OPD) behaviour and the relationship with the fabric dynamic permeability (DP), as the complete understanding of the mechanism from fabric OPD to fabric DP will be desirable for optimum design of such technical textiles and exploration of their new applications.

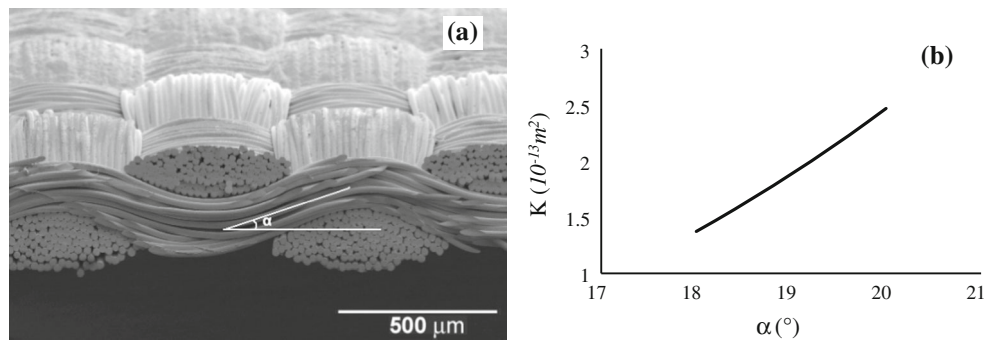
As known, 2D woven fabric is a flexible, discontinuous and anisotropic sheet, and can be easily deformed by an out-of-plane pressure load, which may involve fabric nonlinear tensile, shear, bending and compression behaviours. Hursa [1] used a fabric unit-cell geometrical model to predict the OPD with its micromechanical tensile, which may contribute to the link of fabric deformation to DP. King et al. [2] proposed a continuum constitutive model for predicting fabric mechanical behaviour in-planar direction. The approach relied on the selection of a geometrical model for the fabric weave, coupled with constitutive models for the yarn behaviours. The structural configuration was related to the macroscopic deformation through an energy minimisation method. This method is useful as it covers all aspects of mechanical properties in the fabric OPD. Lin et al. [3] developed an analytical model for the OPD of a square textile composite by its own weight. Trigonometric functions were used to describe the in-plane and out-of-plane displacements of any point. Energy minimisation approach was employed to analyze the composite

X. Xiao (✉)
Institute of Textiles and Clothing, The Hong Kong Polytechnic University, Hung Hom, Hong Kong
e-mail: xiao_xueliang@163.com; xueliang.xiao@polyu.edu.hk

A. Long · X. Zeng
Division of Materials, Mechanics and Structures, Faculty of Engineering, University of Nottingham, University Park, Nottingham NG7 2RD, UK

Table 1 Transverse permeability (K_{\perp}) of yarns developed by a few researchers

Researcher	Hexagonal	Quadratic
Gebart [4] Eq. 1	$K_h = \frac{16}{9\pi\sqrt{6}} \left(\sqrt{\frac{\pi}{2\sqrt{3}V_f}} - 1 \right)^{2.5} \cdot R_f^2$	$K_q = \frac{16}{9\pi\sqrt{2}} \left(\sqrt{\frac{\pi}{4V_f}} - 1 \right)^{2.5} \cdot R_f^2$
Cai [5] Eq. 2	$K_h = 0.07R_f^2 \cdot \left(\frac{1 - \sqrt{\frac{V_f}{0.907}}}{\frac{V_f}{0.907}} \right)^{2.5}$	$K_q = 0.12R_f^2 \cdot \left(\frac{1 - \sqrt{\frac{V_f}{0.785}}}{\frac{V_f}{0.785}} \right)^{2.5}$
Bruschke [6] Eq. 3	$K_h = \frac{R_f^2 (1-l^2)^2}{3\sqrt{3}} \cdot \left(3l \frac{\arctan(\frac{\sqrt{1-l^2}}{l})}{\sqrt{1-l^2}} + \frac{l^2}{2} + 1 \right)^{-1}$	$K_q = \frac{R_f^2 (1-l^2)^2}{3} \cdot \left(3l \frac{\arctan(\frac{\sqrt{1-l^2}}{l})}{\sqrt{1-l^2}} + \frac{l^2}{2} + 1 \right)^{-1}$
Westhuizen [7] Eq. 4	$K = R_f^2 \cdot \frac{\pi(1-V_f^*)}{24(V_f^*)^{1.5}} (1 - \sqrt{V_f^*})^2$ $V_f^* = 2.22(V_f)^2 - 1.22V_f + 0.56$ ($V_f \geq 0.5$) $V_f^* = V_f$ ($V_f < 0.5$)	$l^2 = \frac{2\sqrt{3}(1-\Phi)}{\pi}$ $l^2 = \frac{4(1-\Phi)}{\pi}$

**Fig. 1** a Cross-section of tight fabric, b relationship of permeability (K) and crimp angle (α)

tensile, shear, bending and exerted external force. The predictions for the maximum deflections of a few weave composites showed good agreement with corresponding finite element simulations.

Fabric permeability (K) is a measure of the fabric ability to transmit fluids and determined by the fabric geometrical parameters, such as porosity (Φ), fibre radius (R_f) and fabric thickness (L). For tight fabric under a certain pressure drop, fluid has to flow through the space around fibres in overlapping yarns. Hence the fabric permeability can be viewed as equivalent of its yarn permeability. Fibre volume fraction (V_f), R_f and fibre array (usually hexagonal and quadratic) are the key factors in characterising the yarn permeability. Table 1 gives a few analytical models for the relationship of K and the above geometric parameters, where K means a static value based on a specific fabric structure. In Table 1, Eq. 2 is for an equivalent homogeneous medium based on a self-consistent approach while Eqs. 3 and 1 are from lubrication solution. Equation 3 suits for high porous materials, but Eq. 1 handles high dense media. In addition, Eq. 1 expresses fluid flow through unidirectional multi-filaments with circular cross-section but Eq. 4 describes flow through filaments with square cross-section. Herein Eq. 1 is selected for predicting the transverse permeability of fibre bundles in this article.

Moreover, Gebart developed one more equation for flow along unidirectional fibres (K_{\parallel}):

$$K_{\parallel} = \frac{8R_f^2 (1 - V_f)^3}{c V_f^2} \quad (5)$$

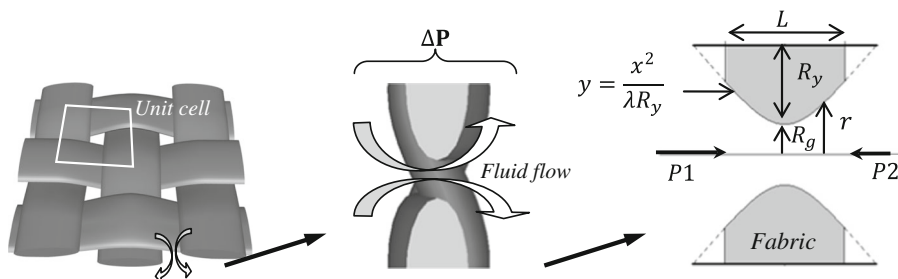
Value for c is 57 when fibre array is quadratic and 53 for hexagonal. However, yarns are undulated in fabric, as shown in Fig. 1a, leading to the increased fabric permeability. Advani [8] introduced an expression (Eq. 6) according with this situation:

$$K = K_{\parallel} \sin^2 \alpha + K_{\perp} \cos^2 \alpha - \frac{(K_{\perp} - K_{\parallel})^2 \cos^2 \alpha \sin^2 \alpha}{K_{\parallel} \cos^2 \alpha + K_{\perp} \sin^2 \alpha}, \quad (6)$$

where α is the maximum crimp angle between the yarn axis and the in-plane direction of fabric as shown in Fig. 1, K_{\parallel} and K_{\perp} are the permeabilities along (Eq. 5) and perpendicular (Eq. 1) to the fibre axis, respectively. Equation 6 shows an increase of α leads to the total fabric permeability increase, as shown a calculation example in Fig. 1b.

For loose fabric with clear gaps between yarns, majority of fluid would flow through the gaps under a certain pressure drop. Gap radius (R_g), yarn width (R_y), fabric thickness (L) and shape factor of flow channel (λ) determine the fabric

Fig. 2 Parabola for boundary shape of flow channel between two yarns in a unit cell of woven fabric



permeability. Kulichenko [9] developed an analytical model for flow through the gaps assuming the gaps are parallel capillaries. Without λ , the model gives more than 60 % error compared with the experimental fabric permeability. Xiao et al. [10] developed an analytical model for the static through-thickness permeability of woven fabric based on the work of Gebart [4], Phelan and Wise [11] and Kulichenko [9]. By defining R_g and R_y within hydraulic diameter, λ by a parabolic equation, there are

$$R_g = \frac{(C_j - D_j)(C_w - D_w)}{C_j - D_j + C_w - D_w} \tag{7a}$$

$$R_y = \frac{C_j C_w}{C_j + C_w} - R_g \tag{7b}$$

$$y = \frac{x^2}{\lambda R_y} \tag{7c}$$

where D_w and D_j are the widths of weft and warp yarns, while C_w and C_j are the spacings of weft and warp yarns, respectively. A simplified diagram for this model is shown in Fig. 2.

This model was developed based on the Poiseuille flow theory and can be used for static permeability prediction for fabrics with clear gaps between yarns, i.e. loose fabrics. It was shown a close prediction with less than 15 % error compared with experimental data

$$K = \frac{2R_g^4}{5\pi} \frac{L}{\sqrt{\lambda R_g R_y} \cdot (R_g + R_y)^2} \tag{8}$$

This paper takes into account the fabric deformation under out-of-plane uniform loading (OPUL), and the effect on the fabric geometric parameters. The fabric DP is thereafter calculated based on the varying geometrical factors. Two typical fabrics (tight and loose) are used to make the experimental verifications. Results and discussions are given, following with the conclusions finally.

Analytical modelling

Fabric deformation under OPUL

Fabric behaviour under OPUL is modelled through assuming an originally flat, stress-free circular fabric

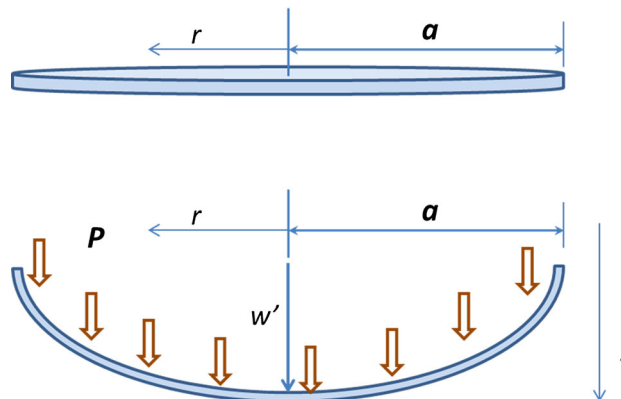


Fig. 3 Schematic of geometry and polar coordinates for a deformed circular fabric

sample with axisymmetric deformation. Polar coordinates are used in this particular deflection case.

Figure 3 is the schematic diagram of a clamped circular fabric at free-state and its deflection under loading by side view. The origin of polar coordinates is placed at the centre of the fabric, giving the fabric radius a . r and z represent in-plane and out-of-plane directions. The boundary conditions in this case are

$$r = 0, u = 0; \quad r = a, u = 0; \tag{9a}$$

$$r = 0, w = w', \frac{dw}{dr} = 0; \quad r = a, w = 0; \tag{9b}$$

where u and w are the displacements in r and z direction, respectively, w' is the maximum displacement in z direction. Due to the symmetric geometry and the uniform loading, it can be concluded that w is an even function of r whereas u is an odd function of r . The requirements can be satisfied by taking the following trigonometric approximations for the displacements:

$$u = c \cdot \sin\left(\frac{\pi r}{a}\right) \tag{10a}$$

$$w = w' \cos\left(\frac{\pi r}{2a}\right) \tag{10b}$$

where c is an arbitrary constant. Note that the shape of Eq. 10 is different with the approximation Eq. 11 which exhibits less gradual deflection near the edge of clamped

area [12], which is suitable for a continuous and rigid deformed sheet

$$w = w' \left(1 - \frac{r^2}{a^2}\right)^2, \quad (11a)$$

$$u = r(a - r)(c_1 + c_2 r), \quad (11b)$$

where c_1 and c_2 are factors depending on the boundary conditions. Similarly with Eq. 11, the modelling of the fabric deflection reduces to derivation of the coefficients c and w' in Eq. 10. The coefficients can be determined by the principle of virtual displacements. Under the OPUL, three types of fabric energy occur during the deformation: bending energy U_b , strain energy U_m and loading work done W . Bending energy (U_b) in polar coordinates is defined as

$$U_b = \frac{\mathbf{D}}{2} \iint_0^A \left\{ \left(\frac{\partial^2 w}{\partial r^2} + \frac{1}{r} \frac{\partial w}{\partial r} + \frac{1}{r^2} \frac{\partial^2 w}{\partial \theta^2} \right)^2 - 2(1 - \nu) \frac{\partial^2 w}{\partial r^2} \left(\frac{1}{r} \frac{\partial w}{\partial r} + \frac{1}{r^2} \frac{\partial^2 w}{\partial \theta^2} \right) + 2(1 - \nu) \left(\frac{1}{r} \frac{\partial^2 w}{\partial r \partial \theta} - \frac{1}{r^2} \frac{\partial w}{\partial \theta} \right)^2 \right\} r dr d\theta, \quad (12)$$

where A is the test area, ν is the Poisson's ratio. The Eq. 12 for the deformed circular fabric can be reduced to a simple form due to the axisymmetric bending

$$U_b = \pi \mathbf{D} \int_0^a \left\{ \left(\frac{\partial^2 w}{\partial r^2} + \frac{1}{r} \frac{\partial w}{\partial r} \right)^2 - \frac{2(1 - \nu)}{r} \frac{dw}{dr} \frac{\partial^2 w}{\partial r^2} \right\} r dr \quad (13)$$

where \mathbf{D} is the fabric flexural rigidity, which does not equal to $\frac{EL^3}{12(1-\nu^2)}$ for fabric [3] where E is the fabric Young's modulus. This is due to the fact that the multi-filament structure in fabric bending does not have a mid-plane where its inside is compressed and outside is stretched.

Fabric strain energy (U_m) consists of stretching energy and shearing energy, which plays a pivotal role in the fabric deformation. The expression in polar coordinates is given [12] as follows:

$$U_m = \frac{\pi EL}{1 - \nu^2} \int_0^a \{ \varepsilon_r^2 + \varepsilon_\theta^2 + 2\nu \varepsilon_r \varepsilon_\theta \} r dr, \quad (14)$$

where ε_r , ε_θ are the radial and tangential normal strains. The relationships of strains and displacements are

$$\varepsilon_r = \frac{du}{dr} + \frac{1}{2} \left(\frac{\partial w}{\partial r} \right)^2, \quad (15a)$$

$$\varepsilon_\theta = \frac{u}{r}. \quad (15b)$$

By substitution of Eq. 15 into Eq. 14, the expression of U_m is obtained in the form

$$U_m = \frac{\pi EL}{1 - \nu^2} \int_0^a \left\{ \left(\frac{du}{dr} \right)^2 + \frac{du}{dr} \left(\frac{dw}{dr} \right)^2 + \frac{u^2}{r^2} + \frac{2\nu u}{r} \frac{du}{dr} + \frac{\nu u}{r} \left(\frac{dw}{dr} \right)^2 + \frac{1}{4} \left(\frac{dw}{dr} \right)^4 \right\} r dr, \quad (16)$$

where the component expression $\left(\frac{\pi EL}{1 - \nu^2} \int_0^a \left(\frac{2\nu u}{r} \frac{du}{dr} + \frac{\nu u}{r} \left(\frac{dw}{dr} \right)^2 \right) r dr \right)$ represents shearing energy and the rest is stretching energy.

When the fabric undergoes OPUL, the work done (W) by the loading P per unit area on the fabric from the initial to the equilibrium state is expressed by integrating Pw across the area of the fabric as

$$W = \iint_0^A P w dx dy, \quad (17a)$$

$$W = 2\pi \int_0^a w P r dr. \quad (17b)$$

Therefore the potential energy function (U_{II}) for the clamped fabric under an OPUL contains the bending energy, the strain energy and the work done

$$U_{II} = U_b + U_m - W, \quad (18)$$

where ‘-’ in Eq. 18 represents an external energy to the fabric. In Eq. 18, U_b relates to OPD; U_m links strain energy to the fabric Young's modulus, which concerns with in-plane deformation; W denotes the work done by the uniformly distributed loading.

With the assumed deflected fabric shape (Eq. 10), the first order and the second order of derivatives with respect to r are

$$\frac{du}{dr} = \frac{\pi c}{a} \cos \frac{\pi r}{a}, \quad (19a)$$

$$\frac{dw}{dr} = -\frac{\pi w'}{2a} \sin \frac{\pi r}{2a}, \quad (19b)$$

$$\frac{d^2 w}{dr^2} = -\frac{\pi^2 w'}{4a^2} \cos \frac{\pi r}{2a}. \quad (19c)$$

By substituting Eq. 19 into Eqs. 13 and 16 then integrating over the clamped fabric as well as Eq. 17, the results are

$$U_b = \frac{\pi^3 \mathbf{D} w'^2}{4a^2} \left(\frac{\nu \pi}{2a} + \ln \frac{\pi}{2} \right), \quad (20a)$$

$$U_m = \frac{\pi EL}{1 - \nu^2} \left(\frac{\pi^2 c^2}{4} - \frac{\pi c w'^2}{4a} - \frac{c w'^2 \pi^3}{32a} + \frac{\nu c \pi w'^2}{3a} + \frac{\pi^2 w'^4}{64a^2} + \frac{3\pi^4 w'^4}{1024a^2} + \frac{c^2}{2} \ln 2 \right), \quad (20b)$$

$$W = 4 \left(1 - \frac{2}{\pi} \right) P w' a^2. \quad (20c)$$

In Eq. 20b, the condition $\frac{\partial U_m}{\partial c} = 0$ that can make U_m a minimum that leads to

$$c = \left(\frac{3\pi w'^2 - 4v\pi w'^2 + \pi^3 w'^2}{12a} + \frac{\pi^3 w'^2}{32a} \right) / \left(\frac{\pi^2}{2} + \ln 2 \right). \tag{21}$$

Inserting Eqs. 21 and 20 into Eq. 18 with a numerical calculation

$$U_{II} = \frac{0.52 + v - 0.3v^2}{1 - v^2} \frac{ELw'^4}{a^2} + \frac{(2.8344 + 3.87v)Dw'^2}{a^2} - 1.4535Pw'a^2. \tag{22}$$

Then, application of the minimisation theory, $\frac{\partial U_{II}}{\partial w'} = 0$, yields approximate expressions for the maximum deflection (w') and out-of plane displacement (w) in the forms

$$w' \cong a \cdot \sqrt[3]{\frac{1.4535Pa}{EL} \cdot \frac{1 - v^2}{2.08 + 4v - 1.2v^2}} \tag{23a}$$

$$w = a \cdot \sqrt[3]{\frac{1.4535Pa}{EL} \cdot \frac{1 - v^2}{2.08 + 4v - 1.2v^2}} \cdot \cos\left(\frac{\pi r}{2a}\right). \tag{23b}$$

It is noted that here fabric has been viewed as a flexible thin film as the w' value is much greater than the fabric thickness. In this condition, the resistance of the film to bending is negligible and the U_b can be ignored compared with the U_m in calculation.

Permeability of the deformed fabrics

Equation 23 can predict the fabric w' under a certain uniform load. The corresponding length of the deflected profile (l) is integrated across a diameter

$$l = \int_{-a}^a \sqrt{1 + (f'(w))^2} dr \quad (-a \leq r \leq a), \tag{24}$$

where the $f'(w)$ is the derivative of $f(w)$ with respect to r . The strain (ε) along the diameter is calculated

$$\varepsilon = \frac{l - 2a}{2a}. \tag{25}$$

All yarns are assumed with the same ε value in the deformation.

Tight fabric permeability

Yarn cross-section in the tight fabric is assumed lenticular with width D and height h as shown a tight fabric cross-section in Fig. 1a. Figure 4 simulates the change of tight fabric cross-section during OPD.

During the OPD, R_f and D are supposed to be invariable, the h is reduced into h' , as shown in Fig. 4, which has an assumed relationship under a yarn Poisson's ratio 0.5

$$h' = \frac{h}{1 + \varepsilon}, \tag{26}$$

where ε is based on Eq. 25. Yarn V_f is defined as the total area of fibre cross-section divided by the area of yarn cross-section. Therefore, the original V_f value and its deformed value V_f' are expressed as follows:

$$V_f = \frac{nR_f^2}{Dh}, \tag{27a}$$

$$V_f' = \frac{nR_f^2}{Dh'}, \tag{27b}$$

where n is the number of the filaments in a yarn. Then the relationship of V_f' and V_f should be

$$V_f' = V_f(1 + \varepsilon). \tag{28}$$

For the crimp angle (α) in Fig. 4, the values of α and α' are

$$\sin \alpha = \frac{h}{S}, \tag{29a}$$

$$\sin \alpha' = \frac{h'}{S(1 + \varepsilon)}. \tag{29a}$$

The relationship of the deformed α' and the original α is

$$\sin \alpha' = \frac{\sin \alpha}{(1 + \varepsilon)^2}. \tag{30}$$

Substitution of the parameters V_f' and α' into Eqs. 1, 5 and 6 allows the permeability of the deformed tight fabric to be predicted theoretically.

Loose fabric permeability

For the deformed loose fabric, the yarn cross-section is assumed elliptical, the yarn width is also assumed constant. During OPD, the yarn height is decreased, while the yarn length is increased with ε under yarn Poisson's ratio 0.5 (refer to Eq. 26). The enlarged R_g' between yarns is calculated as follows due to the stretched yarn length with ε :

$$R_g' = R_g(1 + \varepsilon). \tag{31}$$

The shape factor (λ) of the flow channel (gap between yarns) in Eq. 8 relates to the fabric thickness (L)

$$\lambda' = \frac{\lambda}{\left(\frac{L}{L'}\right)^2} = \frac{\lambda}{(1 + \varepsilon)^2}. \tag{32}$$

Substitution of the parameters R_g' , h' and λ' into Eq. 8 allows the permeability of the deformed loose fabric to be predicted theoretically.

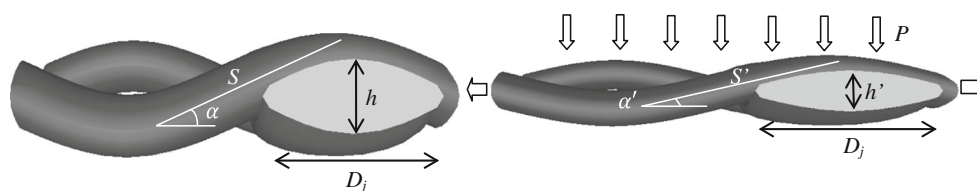


Fig. 4 Geometrical change of fabric cross-section under uniform loading

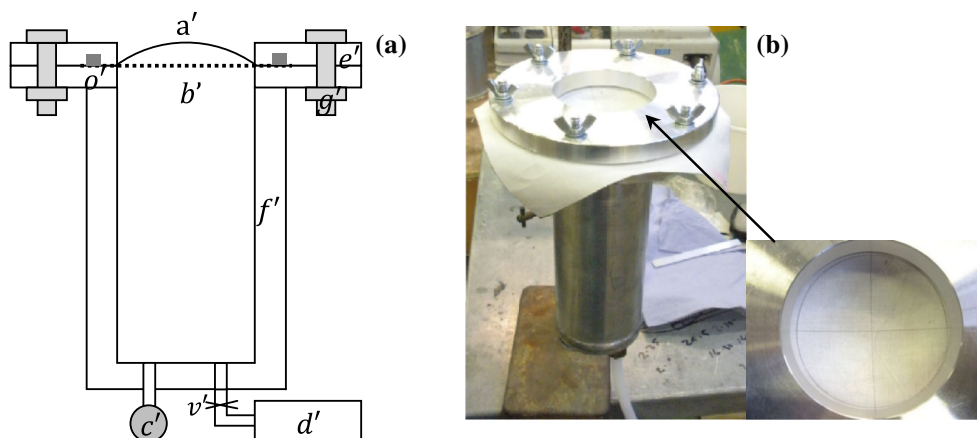


Fig. 5 Fabric deflection tester **a** construction sketch; **b** real tester

Experimental verification

Fabric deformation model

The experimental verification to the model of fabric OPD contains two aspects: the w' and corresponding w . Here a novel experimental device is invented to validate the deformation model.

Design of the fabric deflection tester

Figure 5 shows the design of the fabric deflection tester. In Fig. 5a, a stress-free flat fabric (b') is clamped by two plates (e') with six bolts (g'). The fabric edge is sealed by a compressed rubber ring (o') in plates. The testing diameter of the fabric in this device is 82 mm. A larger of cling film (a') is in place to ensure the system is airtight. The size of the film is slightly greater than that of the fabric to avoid influence on fabric deformation. The air in the container (f') is pumped by a vacuum pump (d'). There is a valve (v') that can control the vacuum level in the container. A vacuum pressure gauge (c') gives the pressure reading inside the sealed container.

The device is designed to produce a vacuum pressure up to 100 kPa. A steel ball with diameter of 4 mm is used to determine the place of w' . A ruler is placed on the top plate across a diameter parallel to the fabric warp, weft and 45° of warp/weft directions, respectively. A vernier caliper is

placed on the ruler perpendicularly and movable to determine the displacement of the fabric deflection. Each fabric deflection under a certain pressure load was repeated five times for the three directions with a fresh sample. Average fabric deflections for the repeats were given with standard deviations.

Experimental materials

The top views of two woven fabrics are shown in Fig. 6 and their specifications are listed in Table 2. The fabric L was determined using the FAST-1 (Fabric Assurance by Simple Testing) device developed by CSIRO. A compression pressure of 196 Pa was applied to the fabric during the measurement [13]. Fabric images were obtained using a ZEISS AxioScope A1 microscope. The images were used to measure C (distance between yarn centre lines), D and α by a free image analysis software Image-J [14]. It is noted that Fabric A_1 represents a tight fabric with no gaps between yarns. The yarns in Fabric A_1 are made of multi-filaments without any twist. In contrast, Fabric U_2 is a loose fabric with clear gaps. The yarns in this fabric are made of 65 % PET and 35 % cotton staple fibres, which are 'Z' spinning with twist of 858/m.

Fabric Young's modulus (E) and flexural rigidity (D) were both measured by Kawabata Evaluation System (KES) [15]. Two parameters were both tested using samples with size 30×20 cm. In KES, one side of fabric was gripped by

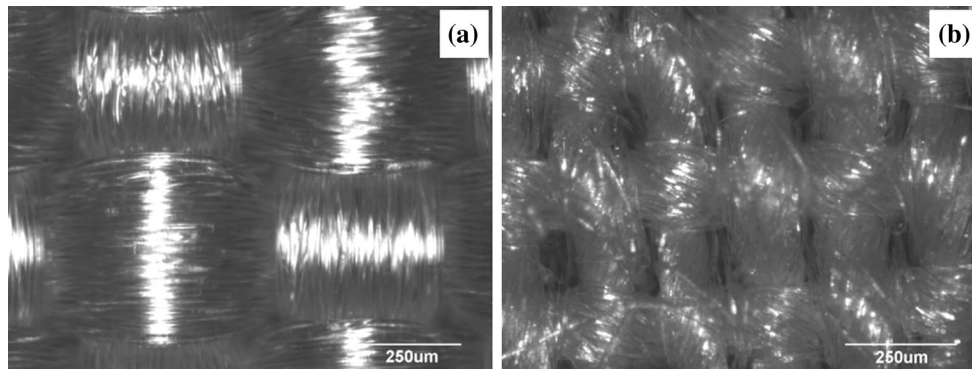


Fig. 6 Fabric structure of **a** Fabric A₁; **b** Fabric U₂

Table 2 Fabric specifications in average values before OPUL (±SD)

Fabric	Composition and structure	R_f mm	Yarn V_f	L mm	α	C mm		D mm	
						Warp	Weft	Warp	Weft
A ₁	100 % Nylon plain	0.34 (±0.01)	0.68 (±0.01)	0.34 (±0.01)	20°	0.53 (±0.02)	0.45 (±0.01)	0.45 (±0.01)	0.52 (±0.01)
Fabric	Composition and structure	Ave λ	L mm	α	C mm		D mm		
					Warp	Weft	Warp	Weft	
U ₂	65 % PET/35 % cotton plain	12.96 (±0.32)	0.32 (±0.01)	14°	0.22 (±0.03)	0.33 (±0.01)	0.17 (±0.03)	0.19 (±0.03)	

two fixed grippers paralleled to its warp or weft yarns while the other side was gripped by movable grippers. If the movable grippers stretch a fabric forward with an increasing load up to 4.9 N, the increased tensile stress (N/mm) and fabric strain (%) were recorded. Its slope divided by L (assumed constant) was the fabric E value with a unit Pa. In Fig. 7, the slope of tensile stress–strain of Fabric A₁ is almost a constant when the strain is less than 10 %. However, the slope keeps increasing for Fabric U₂. The average values of initial E for warp and weft directions are calculated as 247 MPa for Fabric A₁ and 148 MPa for Fabric U₂ when both stains are less than 10 %. If the movable grippers rotate around the fixed grippers with a sample, a relationship of bending moment and fabric curvature was recorded as a closed curve. Slope of the first part of the curve in Fig. 7 is the D value with a unit Nmm. The expression $\frac{EL^3}{12(1-\nu^2)}$ was calculated as 889×10^{-6} Nm for Fabric A₁ and 444×10^{-6} Nm for Fabric U₂ based on the measurements of E , L and $\nu(0.5)$ for both fabrics, which are much larger than the corresponding measured D values 66.4×10^{-6} Nm for Fabric A₁ and 7.85×10^{-6} Nm for Fabric U₂ from Fig. 7. This proves that the equation $D = \frac{EL^3}{12(1-\nu^2)}$ for continuous solid plates does not suit for textile fabrics.

An attempt was made to measure ν values of the two fabrics using Digital Image Correlation (DIC) equipment according to Hursa’s approach [16], however, the results showed both larger than 1 which is not considered

physically realistic. In the next section, a few ν values will be used to assess sensitivity.

Deformed fabric permeability measurement

The fabric through-thickness K without deformation was measured by a Shirley Air Permeability Tester. The air pressure drop is 300 Pa. The test area is 5.07 cm^2 (1 inch²) and the airflow rate is in the range of 0.1–350 cm³/s. Each fabric was tested five times. The K value was calculated according to Darcy’s law

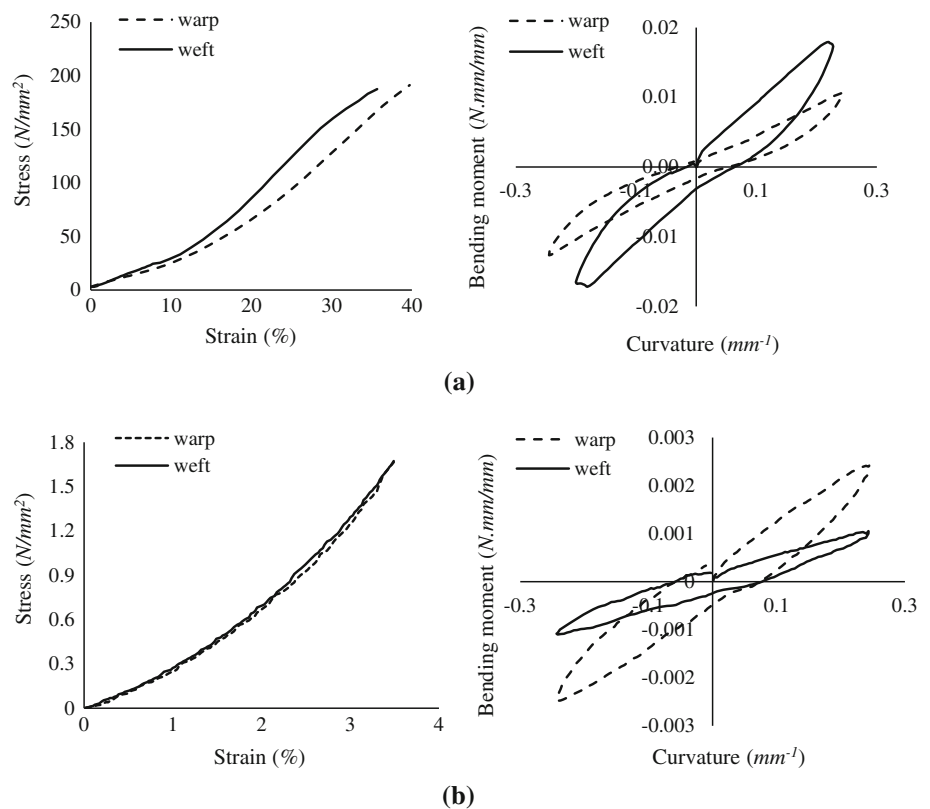
$$\frac{P}{L} = \frac{\mu V}{K} \tag{33}$$

where μ is the gas viscosity and V is the average gas velocity. The fabric through-thickness K value during the OPD was measured by a ‘dynamic permeability tester’, which was designed and constructed by Leeds University. More details about the working principle of the tester can be found in Bandara et al. [17] or Xiao et al. [18]. The tester provides a circular test area of 50 cm^2 . The test pressure is in the range of 5 and 300 kPa above atmospheric pressure. For the two fabrics, the initial uniform loading of 80 kPa was applied. The K value was obtained by the Forchheimer equation

$$\frac{P}{L} = \frac{\mu}{K} V + \beta \rho V^2, \tag{34}$$

where ρ is the gas density, β is the non-Darcy coefficient.

Fig. 7 Tensile stress–strain and bending moment–curvature relationships of fabrics obtained by KES **a** Fabric A₁; **b** Fabric U₂



Results and discussions

Fabric deformation model

Maximum displacement

The maximum displacement (w') of fabric occurs at the centre of the test area under OPUL. The prediction is based on Eq. 23a, assuming three ν values (0.2, 0.3 and 0.4) in the range for woven fabric [16, 19]. The comparisons of w' between predictions ('Pred' curves) and measurements ('EXPT' dots) are shown in Fig. 8.

With a fixed ν value, the predicted w' is proportional to the cubic root of the OPUL (P) according to Eq. 23a. The 'EXPT' dots in Fig. 8 show a nonlinear relationship of w' and P which is close to the cubic root relationship in the prediction. The graphs also show that a smaller ν value can obtain a higher prediction of w' , and the interval between $\nu = 0.2$ and 0.3 is much less than that of 0.3 and 0.4, showing the relationship of w' and ν values is nonlinear. The comparisons show the ν value for Fabric A₁ is close to 0.3 while Fabric U₂ is close to 0.2. In the graph, the w' value for Fabric A₁ is smaller than that for Fabric U₂ at the same loading. The reason is a smaller stiffness value of Fabric U₂.

Deflection profile

Figure 9 compares the experimental measurements of fabric deflection based on the average value for three directions along a diameter with the predictions based on Eqs. 10 and 23b (the curves 'Pred' in Fig. 9). The 'Eq. 11 Pred' profile in Fig. 9 is based on Eq. 11 which assumes the displacement equations are polynomials. The fabric deflections in Fig. 9 are both under the same uniform loading of 100 kPa, where the w' values are found of 1.1 cm for Fabric A₁ and 1.28 cm for Fabric U₂. This gives the strain ε values of 3.6 % for Fabric A₁ and 6.6 % for Fabric U₂ according to the Eqs. 24 and 25. It is evidently practicable of the E values obtained from Fig. 7 for the fabric deformation prediction. Here the ν values for predictions are 0.3 for Fabric A₁ and 0.2 for Fabric U₂. The experimental results prove the approximations (Eq. 10) for the fabric deflection are reasonable and more accurate than that from Eq. 11. The difference in the predictions based on between Eqs. 11 and 10 is mainly displayed in the deflected profile near the clamped area. The prediction of Eq. 11 show the vertical displacement declines slowly in this area due to the polynomial nature, and Eq. 10 shows a steep deflection in contrast due to the cosine function.

Fig. 8 Fabric maximum displacements during out-of-plane uniform loading **a** Fabric A₁; **b** Fabric U₂

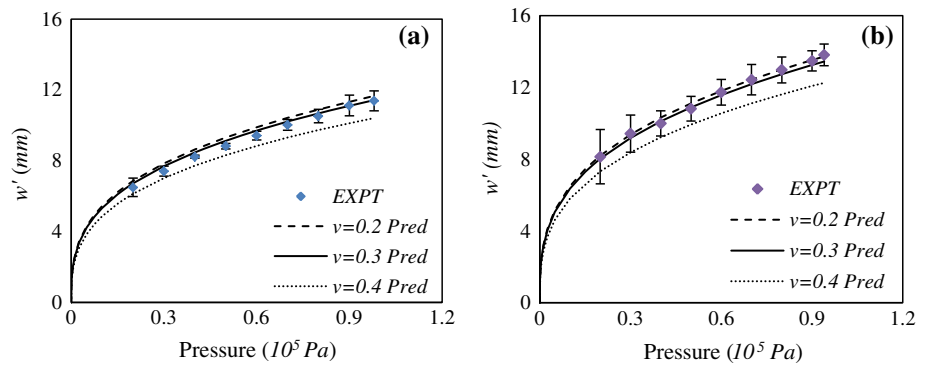


Fig. 9 Comparison of experimental measurements against predictions of fabric deflection along diameter (*Error bars* represent standard derivation based on five repeats of tests at each point)

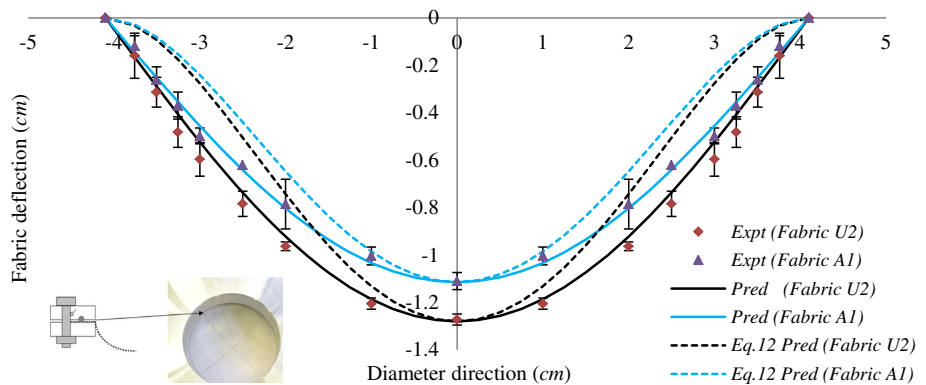


Figure 10 shows the deflected profiles of Fabric A₁ along the same diameter under different OPULs. It is easier to deform at low loading due to the yarn crimp of interwoven structure of the woven fabric. A greater OPUL achieves less increased displacement because the loading is now undertaken by yarns in the in-plane direction.

Permeability model of deformed fabric

Tight fabric A₁

Figure 11 shows the V_f and α values are strongly influenced by OPUL. An increase in loading causes V_f to increase and α to decrease. One reason might be the increased contact force at yarn cross-overs, which pushes fibres together in a tighter bundle. Figure 11 also shows a smaller ν value causes yarns to exhibit a larger V_f value.

Figure 12 compares the fabric K prediction ($\nu = 0.3$) with experimental results under three OPULs. More details on experimental data processing can be found in Xiao’s work [18]. The average tested values consist of one static and two dynamic permeabilities. As shown in Fig. 12, the predictive model agrees with the experimental results very well. The K value is decreasing with the increase of OPUL for tight fabric. The essential reason is that V_f is increased due to the reduced h by increasing loading on fabric.

Loose fabric U₂

Table 2 offers initial values of C and D , which can be transferred into R_g and R_y by Eqs. 7a and 7b. Due to the OPUL, the fabric deflection leads to an increase in the fabric surface area. Yarns tensioning causes an increase in R_g and a decrease in L and λ .

The similarity of Fig. 13 with Fig. 11 is due to the same basis of the Eqs. 23–26. In Fig. 13, R_g shows a nonlinear relationship with OPUL. An increase of the loading causes an increase of R_g from Eq. 31. Substituting Eqs. 31 and 32 into Eq. 8, L and λ are eliminated, therefore, there is no need to compare the effect of loading on the two geometrical factors L and λ . Fig. 14 shows K is increasing as R_g is enlarged when the loading on the fabric increases. In the prediction, yarn permeability was ignored. The model predicts with reasonable accuracy for the relationship of permeability and loading in the test range. However, under the high OPUL, the model gives an underestimated prediction. The reason might be the limitation of Eq. 8 as it was obtained from Darcy’s law. The relationship of pressure drop and fluid velocity is nonlinear when the velocity reaches a particular high range. The Forchheimer equation (Eq. 34) should be used for prediction of flow behaviour in this range.

Fig. 10 Deflection profiles of Fabric A₁ under different uniform loadings

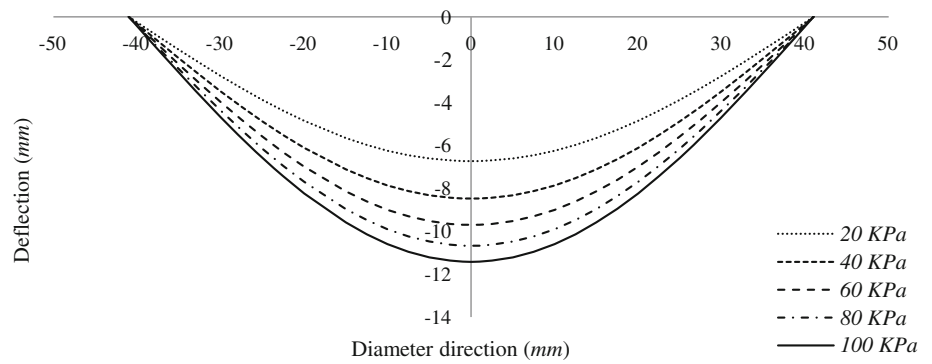


Fig. 11 Effect of uniform loading on the parameters of V_f and α

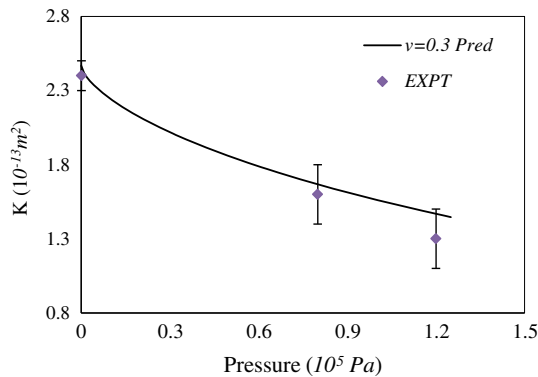
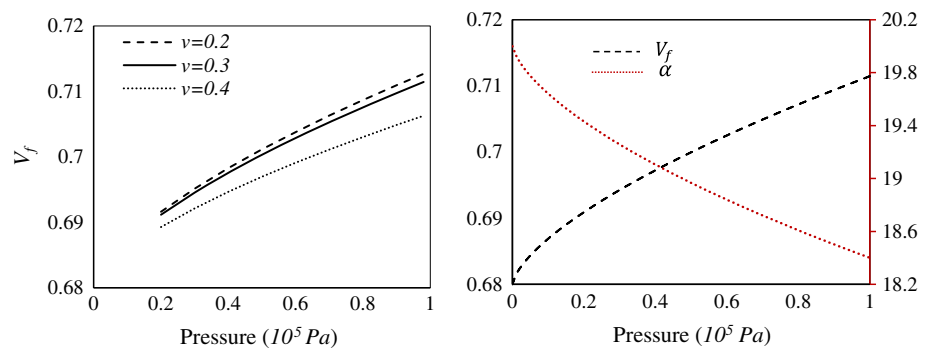


Fig. 12 Comparison of permeability prediction with experimental data under increasing loadings

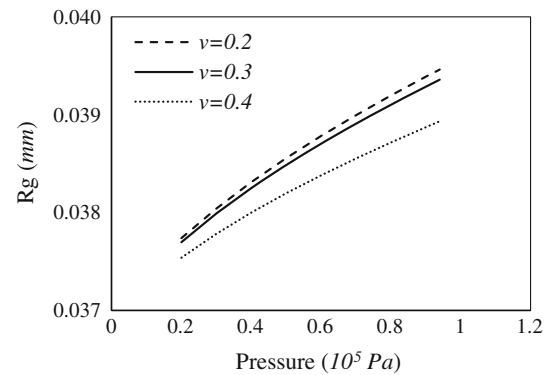


Fig. 13 Effect of pressure load on R_g

Sensitivity study

The current model shows how to predict the through-thickness K of a woven fabric under certain OPUL. During the deformation, Φ which is defined as the gap area divided by the fabric area, and L are the most sensitive parameters influenced by the loading. For loose fabric, K under the loading is increased due to the increase of Φ . For tight fabric, K is reduced by decreasing L . Figure 15 investigates the sensitivity of Φ and L to the K when fixing other specifications of Fabric U₂ under OPULs. Figure 15a shows the critical Φ value is in the range of 0.5 and 0.6 %

which is much smaller than its original value 5.04 % based on the specifications in Table 2. When Φ is higher than 0.6 %, K gets larger under OPULs. While Φ is lower than 0.5 %, the trend of K is opposite. When the Φ value is 0.53 % (critical value), increasing L gives a larger K value under the loading as shown in Fig. 15b, and vice versa.

Apart from Φ and L , fabric E , ν and radius (a) also relate to the final fabric K value. Herein, the effects of E and a on this relationship are discussed. Figure 16a shows an increase of E for tight fabric results in an increase of K . The reason is that the fabric deflection is decreased as E increases. Thereafter, the yarn V_f decreases as discussed in “Tight fabric A₁” section (Eq. 28), leading to a higher

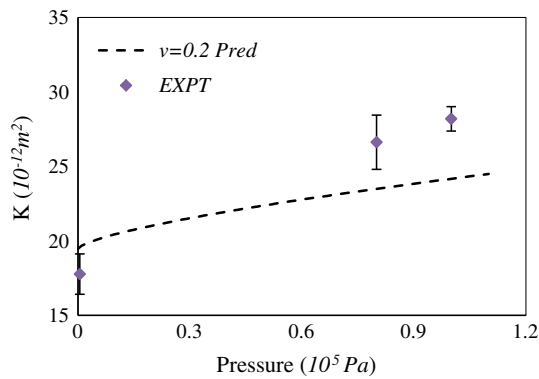


Fig. 14 Comparison of permeability prediction and experimental values under increasing OPULs for Fabric U₂

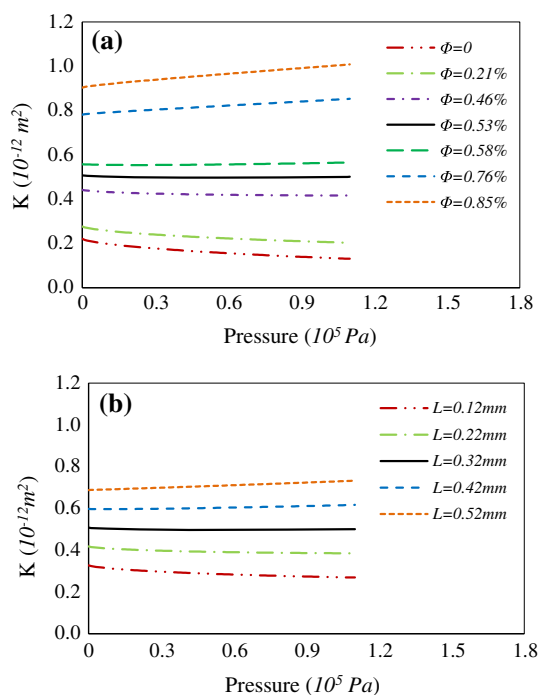


Fig. 15 Effects of **a** original fabric porosity (Φ) and **b** original fabric thickness (L) on the relationship of K and P (Fabric U₂)

K . However, the increase of K is nonlinear with the increase of E . It shows K is decreased with an increase of loading for a fixed E value. In Fig. 16b, loose fabric has the opposite trend compared with tight fabric. The R_g is increased as E is decreased, leading to a larger K value (Eq. 8).

Figure 16 also shows the relationship by changing a when other parameters are fixed. An increase of a will increase the w' value of the deformed fabric (Eq. 23a) and ϵ value (Eqs. 24, 25), influencing the final K value. Figure 16a shows that K is decreased with increasing a as V_f is increased for tight fabric. The difference of K values

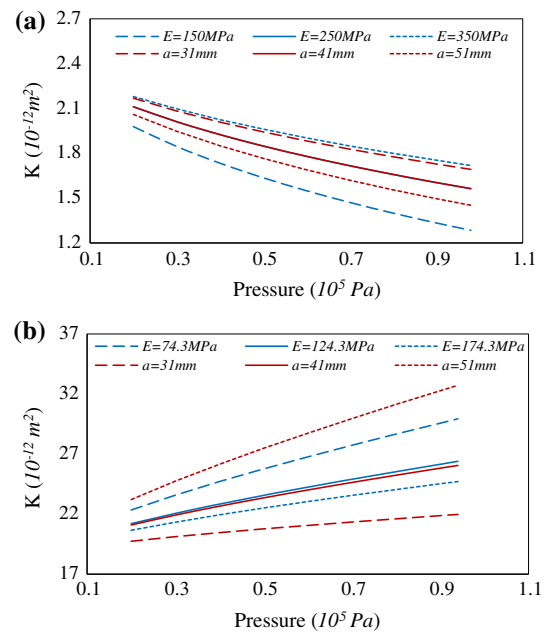


Fig. 16 Effect of E and a on the relationship of K and P **a** tight fabric; **b** loose fabric

between $a = 41$ mm and $a = 51$ mm is smaller than that of $a = 31$ mm and $a = 41$ mm, indicating a lower effect of increased a on decreasing the K value. Figure 16b shows K of loose fabric is increased as its a value increases. The reason might be that R_g is getting larger relatively as the fabric is deformed more at a larger a value. The difference of K values between $a = 31$ mm and $a = 41$ mm is smaller than that of $a = 41$ mm and $a = 51$ mm, indicating that an increase of a will cause the fabric K to increase further.

Conclusions

Three analytical models were proposed for predicting the OPD of woven fabric under perpendicular uniform loading, and corresponding through-thickness permeability of tight weave and loose weave, respectively. The whole models in this paper contribute to the mechanism understanding the effect of external factors on the fabric dynamic permeability, and assists with optimum design of technical textiles in the OPD working environment.

In the modelling of fabric OPD under a uniform load, an energy-based approach was utilised to predict bending energy, strain energy and external energy. The fabric was assumed to behave like a thin film based on the membrane large deformation theory. Minimisation energy of the system was used to derive the relationship of the maximum displacement and the loading. Fabric-deflected shape was characterised by the displacement and a cosine function of the fabric radius. The model for predicting the permeability

was based on the accurate prediction of the fabric deformation. Also, it relied on the accurate prediction of the static permeability (Eqs. 1, 5, 6, 7, 8). The assumption was that the yarn width was invariable during the deformation. Fabric thickness was reduced with the same rate of yarn height. Tight fabric permeability was predicted through the increased yarn fibre volume fraction and crimp angle due to the decreased yarn height. Loose fabric permeability was predicted by the increased gap radius due to the enlarged fabric area caused by fabric deflection.

Three kinds of experiments were used to verify the analytical predictions. Fabric OPD was measured by a fabric deflection tester, with loading applied by a vacuum pump. Fabric static permeability was determined by a Shirley air permeability tester while fabric dynamic permeability was tested by a dynamic permeability tester. The predictions for the fabric deflection configurations (tight and loose fabrics) agree with the experimental measurements very well. The deflection causes the yarn fibre volume fraction and the crimp angle to increase, resulting in the permeability of tight fabric to decrease (Fig. 12). In contrast, the deflection leads to the gap radius to increase, obtaining an increased permeability of loose fabric (Fig. 14). The permeability predictions for the deformed fabrics agree with the experimental values well. Sensitivity studies first, investigate the critical fabric porosity and the critical fabric thickness where the increase or decrease of fabric permeability occurs during the fabric deformation. Second the fabric properties, such as Young's modulus, affect the fabric deformation. An increase of modulus leads to the increase of tight fabric permeability and a decrease of loose fabric permeability when the fabric is under the same pressure load.

Acknowledgements The authors would like to thank Airbags International Ltd. for providing experimental materials, Leeds University and UK Unilever Resources Centre for undertaking the experimental tests.

References

1. Somodi Z, Rolich T, Hursa A (2010) Micromechanical tensile model of woven fabric and parameter optimization for fit with KES data. *Text Res J* 80(13):1255–1264

2. King MJ, Jearanaisilawong P, Socrate S (2005) A continuum constitutive model for the mechanical behavior of woven fabrics. *Int J Solids Struct* 42:3867–3896
3. Lin H, Clifford MJ, Taylor PM, Long AC (2009) 3D mathematical modeling for robotic pick up of textile composites. *Compos B* 40:705–713
4. Gebart BR (1992) Permeability of unidirectional reinforcements for RTM. *J Compos Mater* 26(8):1101–1133
5. Cai Z, Berdichevsky AL (1993) An improved self-consistent method for estimating the permeability of a fiber assembly. *Polym Compos* 14(4):314–323
6. Brusckhe MV, Advani SG (1993) Flow of generalized Newtonian fluids across a periodic array of cylinders. *J Rheol* 37(3):479–497
7. Westhuizen JV, Plessis JPD (1996) An attempt to quantify fibre bed permeability utilizing the phase average Navier–Stokes equation. *Compos A* 27A:263–269
8. Advani SG, Brusckhe MV, Parnas RS (1994) Resin transfer molding flow phenomena in polymeric composites. In: Advani SG (ed) *Flow and rheology in polymer composites manufacturing*. Elsevier, Amsterdam
9. Kulichenko AV (2005) Theoretical analysis, calculation, and prediction of the air permeability of textiles. *Fibre Chem* 37(5):371–380
10. Xiao X, Zeng X, Long A, Clifford MJ, Lin H, Saldaeva E (2012) An analytical model for through-thickness permeability of woven fabric. *Text Res J* 82(5):492–501
11. Phelan JF, Wise G (1996) Analysis of transverse flow in aligned fibrous porous media. *Compos A* 27A(1):25–34
12. Ugural AC (1999) *Stresses in plates and shells*, 2nd edn. McGRAW HILL International editions, Singapore, p 502
13. Ly NG, Tester DH, Buckenham P, Rocznio AF, Adriaansen AL, Scaysbrook F, De Jong S (1991) Simple instruments for quality control by finishers and tailors. *Text Res J* 61(7):402–406
14. Image-J (2012) Available from: <http://rsbweb.nih.gov/ij/features.html>. Accessed on 2012 17/05
15. Chan CK, Jiang XY, Liew KL, Chan LK, Wong WK, Lau MP (2006) Evaluation of mechanical properties of uniform fabrics in garment manufacturing. *J Mater Process Technol* 174(1–3):183–189
16. Hursa A, Rolich T, Razic SE (2009) Determining pseudo Poisson's ratio of woven fabric with a digital image correlation method. *Text Res J* 79(17):1588–1598
17. Bandara P, Lawrence C, Mahmoudi M (2006) Instrumentation for the measurement of fabric air permeability at higher pressure levels. *Meas Sci Technol* 17:2247–2255
18. Xiao X, Zeng X, Bandara P, Long A (2012) Experimental study of dynamic air permeability for woven fabrics. *Text Res J* 82(9):920–930
19. Lu Y, Dai X (2009) Calculation of fabrics Poisson's ratio based on biaxial extension. *J Text Res* 30(9):25–28